Solid Freeform Fabrication 2021: Proceedings of the 32nd Annual International Solid Freeform Fabrication Symposium – An Additive Manufacturing Conference
Reviewed Paper

Accelerated Corrosion Behavior of Additive Manufactured WE43 Magnesium Alloy

Rakeshkumar Karunakaran, Sam Ortgies, Ryan Green, William Barelman, Ian Kobler
Michael Sealy[1]

Mechanical and Materials Engineering Dept., University of Nebraska-Lincoln, Lincoln, NE 68588

Abstract

Magnesium alloys are capable of withstanding the high temperatures and pressures needed in oil and gas fracking operations followed by rapid and complete dissolution in days. Dissolvable magnesium plugs are used in fracking to enable longer lateral wellbores by eliminating mill-outs and the associated debris clogging. To increase extraction efficiency, the key technical challenge is determining how to increase the strength of a high corrosion rate magnesium device that enables higher pressures while maintaining high corrosion rates. Topologically modified dissolvable plugs fabricated by additive manufacturing is proposed as a solution to fabricate high strength and high corrosion rate fracture plugs. Corrosion of magnesium is dependent on surface area exposed to corrosive media and is easily manipulated by additive manufacturing. This study highlights the development of optimal powder bed fusion process parameters for WE43 magnesium alloy and investigates the corrosion behavior of printed WE43 in a salt solution concentrated with sodium bicarbonate to initiate highly accelerated corrosion. Printed WE43 corroded three times faster than an as-rolled sample and was driven by the mechanical and materials properties formed by printing.

Keywords: magnesium, corrosion, powder bed fusion, fracking

1. Introduction

Traditional plugs used in hydraulic fracturing are composed of metal or composite materials. Fracking plugs isolate the lower zones of wellbores during multi-stage high-pressure fracking and are removed by milling after hydraulic stimulation is achieved. Milling of fracking plugs adds to production costs and elevate the risk of milling debris clogging wellbores. Traditional plugs also limit the lateral extension of borewells due to mill-out challenges in lengthy horizontal zones. As a result, there is a need for fully dissolvable fracking plugs [1]. The key barriers to efficient hydraulic fracking using dissolvable plugs are the poor mechanical properties and degradation performance of existing fracking plugs. Degradation rate of commercially dissolvable plugs are currently viable only for 2-mile lateral bores [2]. Dissolvable plugs do not exhibit high degradation rates reliably as required for shorter laterals of 1 to 1.5 miles and still need to be milled to remove. Thus, better dissolvable fracking plugs are required for efficient fracking.

Magnesium (Mg) and its alloys offer a moderate strength metal capable of degrading when in contact with water. Surface area directly correlates to the corrosion rate of magnesium and is a key parameter in developing high corrosion rate (HCR) devices. Additive manufacturing (AM) enables the use of more complex design tools, such as topology optimization, to fabricate

[1] Email sealy@unl.edu | Phone: 402-472-1659

magnesium devices with varying degree of surface area exposed to corrosive environments. Early investigations showed dense printed magnesium corroded, as measured by evolved H_2 gas, at a rate of 5-7 mL/cm^2 over 3 days in 0.1 M NaCl [3] compared to porous magnesium lattices that produced similar amounts of H_2 in 27 days in 5 % fetal bovine serum [4]. These experiments were directed towards biomedical applications and used two different simulated body fluids (*i.e.*, corrosion environments). To the authors' knowledge, there is no literature on corrosion behavior of printed magnesium in highly corrosive environments. Additive manufacturing of magnesium plugs is hypothesized to address the HCR demands of hydraulic fracturing. The target dissolution rate is to have a fracking plug completely degrade in three days.

Commercially available alloys for HCR dissolvable plugs include SoluMag® from Luxfer Mel Technologies and TAx-100E from Terves. The SoluMag® product is a variant of the WE43 alloy system. Thus, AM of WE43 magnesium alloy was conducted in this study to understand corrosion behavior. Salt water generated from fracking is three to six times more saline compared to seawater [5], and several sodium-based acids (accounting for 8 % of the solution) are supplied alongside fracking water to increase productivity [6]. Hence, HCR studies for printed WE43 were conducted in Hank's balanced salt solution with 30X higher concentration of sodium bicarbonate to simulate oil fracking media. This publication adds to the knowledge on revolutionizing smart manufacturing of dissolvable, high-value magnesium tools for the oil and gas industry using three-dimensional printing of HCR devices.

2. Optimizing Additive Manufacturing of Magnesium WE43

2.1 WE43 Powder and Baseplate

WE43 magnesium powder, also known as MAP +43, was obtained from Luxfer Mel Technologies. The WE43 powder was spherical (Fig. 1a) with diameter 28 ± 7 µm (Fig. 1b). Parts were printed on precision ground (± 10 µm) 230 mm × 127 mm × 38 mm baseplates of magnesium alloy ZK-60a. The ZK-60a plates contains zinc and zirconium and is artificially aged at 149°C for 24 hours. This baseplate is stronger and more ductile than WE43 and has a higher thermal conductivity (120 W/mK) compared to WE43 (50 W/mK).

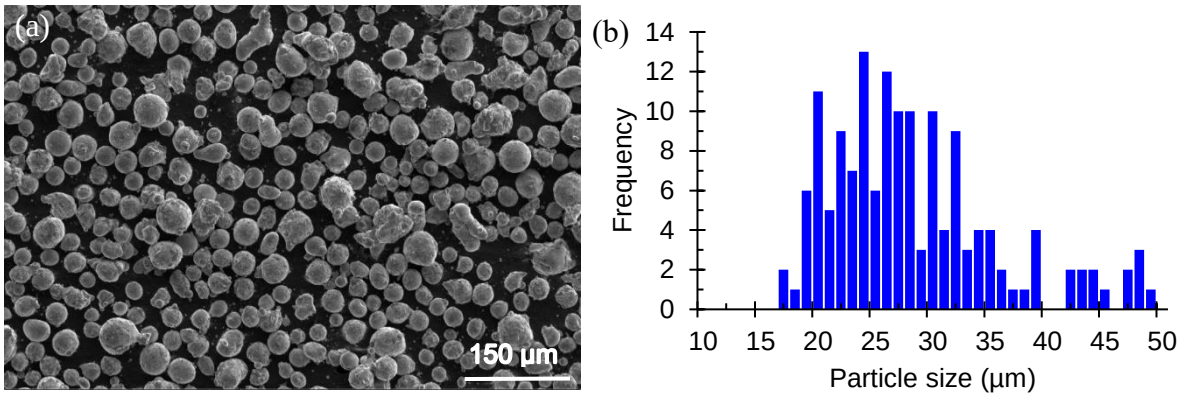

Fig. 1 WE43 powder (a) morphology and (b) particle size distribution.

2.2 Single Track Depositions of WE43

Preliminary experiments were conducted to develop a suitable print recipe by depositing singles tracks using powder bed fusion (PBF) AM in a Matsuura Lumex Avance-25. The Lumex utilizes Yb-fiber laser with a maximum power output of 1000 W and a laser spot size of 0.30 mm. Single tracks 100 mm in length were deposited in an argon atmosphere with less than 1.5 % O_2. The PBF process parameters used for single tracks are listed in Table 1. Single track samples were sectioned off the baseplate and mechanically polished and etched with a 10% nitric acid solution for 5 seconds to reveal meltpool geometry. The meltpool was imaged with an AmScope polarizing metallurgical microscope at 5x magnification. The meltpool width and depth was analyzed using ImageJ software. Meltpool geometry attained from single track depositions was used to identify the optimal process parameter sets to fabricate cubes that yield the highest density. The layer thickness for depositions was 50 µm and the meltpool needed to penetrate approximately 100 µm to fuse adjacent layers. The melt pool also needed to be 150 µm in width to allow for 50% overlap between adjacent rasters that are typically 100 µm in width [8].

Table 1 Process parameters for single tracks on baseplate with and without WE43 powder

Process Parameters	
Laser Power:	100 W, 135 W, 200 W, 350 W
Scan Speed:	500 mm/s, 700 mm/s, 1000 mm/s

A representative image of meltpool attained from single track depositions is shown in Fig. 2. The meltpools attained from single tracks were 100 µm ± 15 µm deep, 150 µm ± 20 µm wide, and showed symmetry about their center axis. No instances of key holing were observed in the depositions. The single tracks also adhered well with the baseplate.

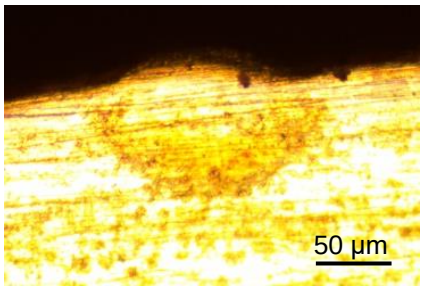

Fig. 2 Meltpool obtained at 135 W laser power and 700 mm/s scan speed.

Increase in laser power yielded larger melt pool while increasing scan speed reduced meltpool size. Low laser powers and high scanning speeds lowered the interaction between the laser and the baseplate, leading to lower meltpool dimensions. The depth and width varied linearly with scan speed and had a cubic relation with laser power. A previous publication noted a parabolic relationship between laser power and width that may be attributed to differences in the PBF

system [9]. Table 2 indicates four sets of single track process parameters that yielded optimal meltpools.

Table 2 Meltpool dimensions for optimal process parameters

Laser power (W)	Scanning speed (mm/s)	Meltpool depth (mm)	Meltpool width (mm)
100	700	0.088	0.163
135	700	0.099	0.160
200	500	0.097	0.167
200	700	0.089	0.165

2.3 Cubes for Density Measurements

Four sets of laser power and scanning speeds were identified from single track depositions that yielded the ideal meltpool dimensions. The parameter sets coupled with three hatch spacings (0.08 mm, 0.10 mm, and 0.12 mm) formed 12 process parameter sets for cube depositions while the layer thickness was maintained at 50 µm. Three cubes were printed for each parameter set for statistical analysis of cube density. Parts were printed from right to left on the baseplate to oppose argon gas flow in the system (Fig. 3). Average density for each set of three cubes was determined using Archimedes principle. Chemical composition and microstructure of the top three parameter sets that yielded highest densities were analyzed on a FEI Helios NanoLab 660.

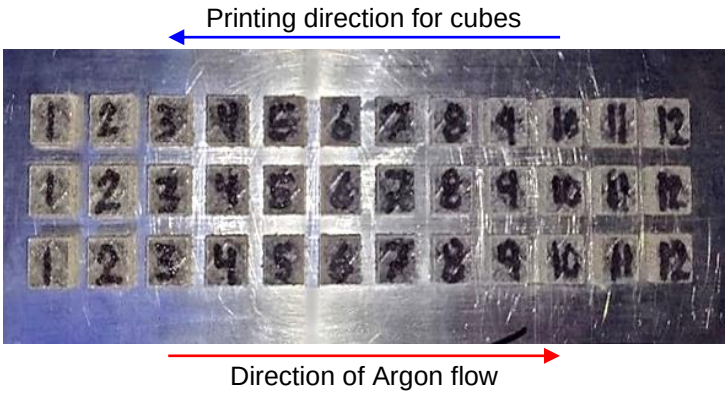

Fig. 3 Cubes for density measurements printed on a baseplate.

The optimal process parameter sets identified from single track depositions were used to print cubes by coupling with three different hatch spacings indicated in Table 3. All printed cubes were at least 96% dense compared to as-rolled WE43 that had a density of 1.845 g/cm^3. Parts printed with laser energy density of 25 to 75 J/mm^3 yielded highest density cubes. Cubes printed with 135 W laser power, 700 mm/s scan speed, and 0.12 mm hatch spacing yielded the highest density of 1.843 g/cm^3 that corresponds to 99.89 % relative density compared to as-rolled WE43.

Table 3 Density of printed WE43 cubes and corresponding laser energy density

Laser power (W)	Scan speed (mm/s)	Hatch spacing (mm)	Laser energy density (J/mm^3)	Density (g/cm^3)
100	700	0.08	35.7	1.764
		0.10	28.6	1.779
		0.12	23.8	1.817
135	700	0.08	48.2	1.819
		0.10	38.5	1.829
		0.12	32.1	1.843
200	500	0.08	100.0	1.798
		0.10	80.0	1.801
		0.12	66.6	1.821
200	700	0.08	71.4	1.806
		0.10	57.1	1.811
		0.12	47.6	1.811

2.4 Microstructural Analysis

Polished surface of printed WE43 was etched using 2 % nitric acid in ethanol before microscopy. Scanning electron microscopy of the highest density printed WE43 showed rose-like grains typical of printed WE43. Flake-shaped yttrium oxide was dispersed within the sample (Fig. 4).

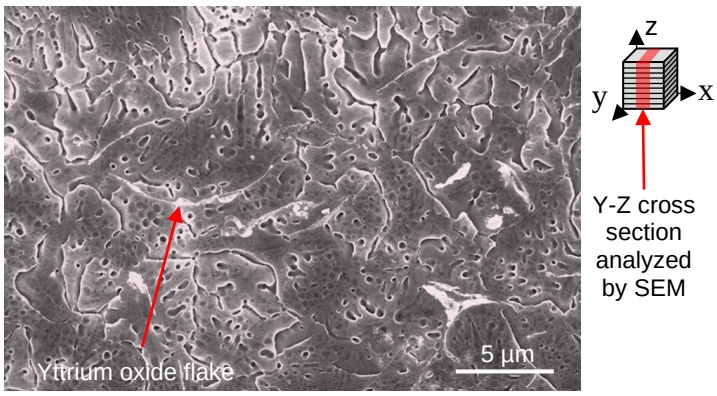

Fig. 4 Microstructure of WE43 printed with laser power of 135 W, scan speed of 700 mm/s, and hatch spacing of 0.12 mm.

3. Corrosion of Printed WE43

An immersion corrosion test (ASTM G31-72 [7]) was used to examine dissolution of WE43. Magnesium reacts in aqueous environments to form magnesium hydroxide ($Mg(OH)_2$) and hydrogen gas, H_2. Magnesium reacts with water to form H_2 in a 1:1 mole ratio that was collected and measured to examine corrosion rate of printed WE43 as a function of time. The corrosion

product $Mg(OH)_2$ is basic and increased the pH of the solution. CO_2 was circulated through the corrosion media intermittently to form carbonic acid and lower the solution pH. The solution was renewed every 2 days and maintained between 7-8 pH throughout experiments.

3.1 Corrosion Sample Preparation

WE43 cylinders 38 mm in diameter and 7 mm in height were printed by PBF using optimal process parameters that yielded the highest density cubes (135 W laser power, 700 mm/s scanning speed, 0.12 mm hatch spacing, and 50 µm layer thickness). Printed samples were separated from the baseplate by a bandsaw, and the parted surface was milled to attain a final sample height of 3 mm. Both parting and milling operations were performed without coolant to avoid corrosion during sample preparation. A 1.5 mm hole was drilled at the center of samples to mount into the immersion setup. Samples were enclosed in epoxy in order to expose only the top surface to corrosion media (Fig. 5). The exposed surface of samples was polished using 150, 320, and 400 grit sandpapers, cleaned with isopropyl alcohol (IPA), and dried. Density of all corrosion samples was measured by Archimedes' method using IPA before immersion tests. Corrosion of printed WE43 was compared with commercially procured as-rolled WE43. The as-rolled samples were also mounted in epoxy and had the same surface preparation as the printed WE43 samples.

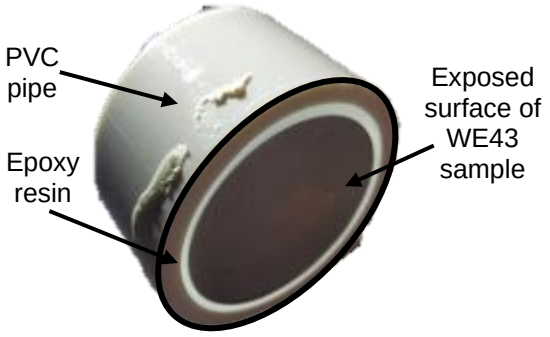

Fig. 5 WE43 sample for corrosion testing.

Samples printed for corrosion studies were larger than samples for previous experiments in this publication. The quality of printed corrosion samples showed dependence on the location within the print chamber unlike prior WE43 prints. Samples printed closer to print chamber door showed delamination compared to parts printed farther away (Fig. 6). Layer delamination was likely due to the directional flow of argon gas inside the print chamber. Soot generated during prints was carried by argon and excessively deposited around samples 1, 2, and 3. Soot has higher carbon content and is thought to have raised the melting temperature of the powder bed around the three samples. The 4^{th} and 5^{th} samples had minimal soot deposition and had higher heat retention while printing due to larger sample size. WE43 has a low melting magnesium alloy that led to WE43 powder vaporization within samples 4 and 5. Weak interlayer bonding due to powder vaporization is suspected to have caused layer delamination. Density of printed samples measured by Archimedes' method showed samples 4 and 5 had 94 % relative density while samples 1, 2,

and 3 had 97 % compared to as-rolled WE43 (Fig. 7). No such delamination was observed for smaller cubes printed earlier to identify optimal process parameters.

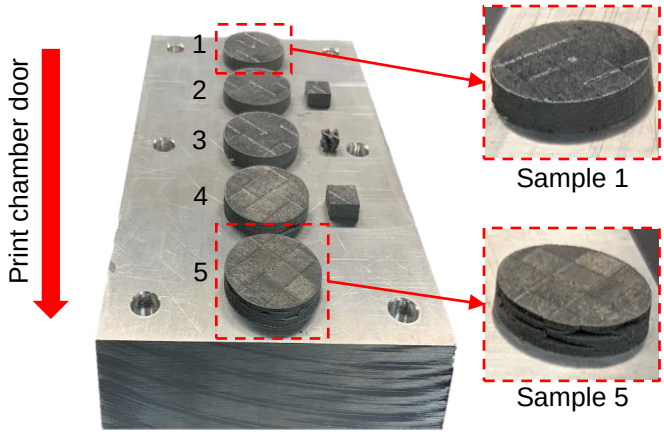

Fig. 6 Printed WE43 corrosion test samples. Samples 1-3 showed no delamination while samples 4 and 5 delaminated.

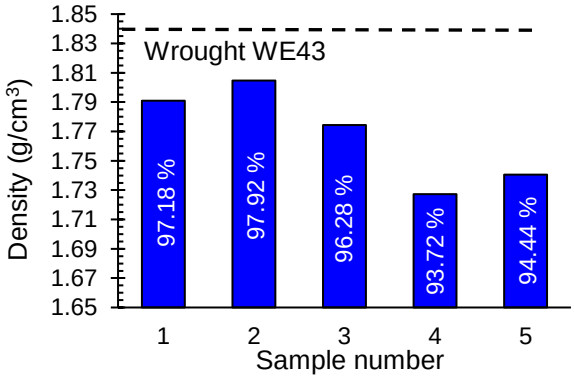

Fig. 7 Dependency of the density of printed WE43 corrosion samples on their position in the print chamber. Percentage values represent relative density compared to as-rolled WE43.

3.2 Immersion Testing – Hydrogen Evolution

A 210 mm × 450 mm × 210 mm glass tank was kept over heating plates for the immersion tests. The tank was filled with Hank's balanced salt solution prepared by adding 10 L of deionized water alongside 97 g of dried Hank's balanced salts (Sigma Aldrich: H1387-10X1L). The solution was doped with 100 g of $NaHCO_3$ as opposed to the recommended 3.5 g to create a concentrated corrosion medium. The corrosion solution was renewed every 2 days and the temperature was set to 37 ºC. Two stir bars rotating at 200 RPM ensured uniform dispersion of salts and temperature in the solution during the immersion tests. Fig. 8 shows the setup for immersion experiments.

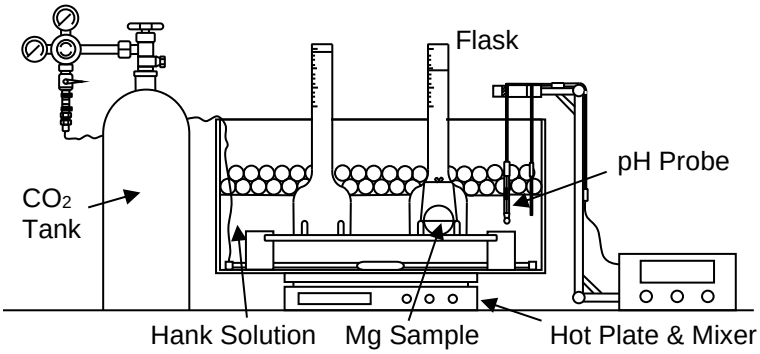

Fig. 8 Experimental setup for corrosion testing.

Samples were placed on a polycarbonate platform at the bottom of the tank, and a graduated beaker was placed above the samples to capture the evolved H_2. A control beaker was placed inside the tank to account for gas bubbles formed due to cathodic hydrogen evolution reaction (reduction of water). Polypropylene hollow balls were added to the tank that floated over the solution to reduce evaporation of the corrosion media. The solution was allowed to heat for 6 to 8 hours prior to corrosion tests to remove dissolved gases before immersion tests. Solution temperature and pH were tracked regularly using a probe (ThermoFisher: 8107BNUMD). CO_2 was supplied at 1 psi when the solution media basicity exceeded 8 pH and was restored to 7 pH. The dispersion of CO_2 was supplied by a diffusion tube with small pores to allow bubbles to form across the entire tank to maximize the interaction within the media. Evolved hydrogen was recorded every 15 minutes during experiments to track corrosion rate.

Immersion experiments on printed WE43 indicated evolved H_2 was highly sensitive to the pH of the corrosion media. Brittle $Mg(OH)_2$ precipitates increased alkalinity of the solution that decelerated corrosion. Hydrogen evolved from printed WE43 accelerated when solution pH was lowered to 7 by suppling CO_2 to the media, while H_2 release plateaued when solution exceeded 7.5 pH (Fig. 9a). A pH dependent H_2 release was also observed for as-rolled WE43, although fluctuations in H_2 evolution due to pH was not as significant compared to printed WE43 (Fig. 9b). The solution alkalinity increased at 0.03 pH/hr. and led to the preferential formation of magnesium carbonate ($MgCO_3$) precipitates at alkalinity higher than 8 pH. The carbonate precipitate formed a thick stable film over the samples and reduced anodic and cathodic interactions of the base metal with the corrosion media, effectively reducing hydrogen evolution from WE43 [10]. Pitting corrosion alongside porosity in printed WE43 increased exposed surface area to corrosive media that drastically accelerated corrosion in the latter portion of the immersion tests for both wrought and printed WE43. Metal AM also accumulate tensile residual stress near surface that creates a favorable environment for accelerated pitting corrosion in printed WE43 [11]. Fluctuations in H_2 evolution due to pH change in the solution smoothened out in the plot (Fig. 10) for corrosion rate. Overall, a 30-fold increase in $NaHCO_3$ resulted a ten-fold increase in H_2 evolution for printed WE43.

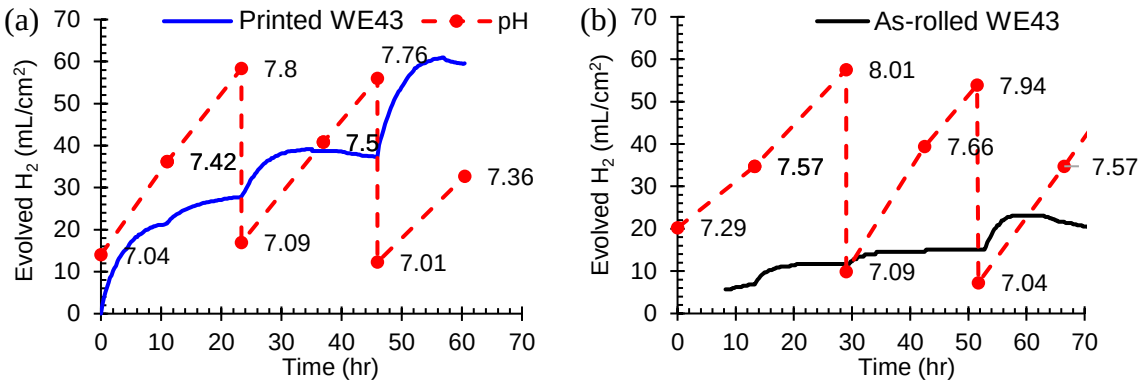

Fig. 9 H_2 evolution in concentrated $NaHCO_3$ solution for (a) printed and (b) as-rolled WE43.

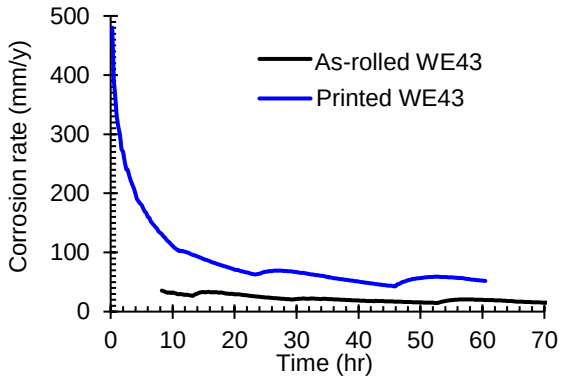

Fig. 10 Corrosion rates of printed and as-rolled WE43 in concentrated $NaHCO_3$ solution.

4. Summary and Future Work

The printability of WE43 magnesium alloy by powder bed fusion was investigated by varying laser power, scanning speed, and hatch spacing. Layer thickness was kept constant at 50 µm for all prints. Highest density cubes (1.843 g/cm^3) were printed at 135 W laser power, 700 mm/s laser scan speed, and 0.012 mm hatch spacing. A relative density of 99.89% was attained compared to as-rolled WE43. A ten-times higher corrosion of printed WE43 was attained in Hank's solution with 30-fold concentrated $NaHCO_3$ compared to non-concentrated Hank's solution. Pitting corrosion was accelerated by porosity and surface tensile stress due to additive manufacturing. H_2 evolution from WE43 during corrosion accelerated at lower alkalinity (7-7.5 pH) and slowed at 7.5-8 pH due to the formation of stable magnesium carbonate films on sample surface. Powder bed fusion printed WE43 corroded three times faster (52.3 mm/year after 60 hours) compared to as-rolled WE43 (19.8 mm/year after 60 hours) in concentrated sodium bicarbonate solution. Future work is to perform accelerated corrosion experiments at higher temperatures to understand the dependence of the cathodic hydrogen evolution reaction on temperature within highly corrosive media. Also, future work will analyze corrosion products to quantify the thickness of magnesium carbonate film on WE43 and its influence on corrosion rate.

Acknowledgements

This research was conducted as part of an undergraduate/graduate investigative research course in additive manufacturing in the Department of Mechanical and Materials Engineering at UNL Spring of 2020. This activity was supported by NSF CMMI: 1846478 and performed in part in the Nebraska Nanoscale Facility (NSF ECCS: 1542182) and Nebraska Engineering Additive Technologies (NEAT) Lab supported by the Nebraska Research Initiative. Matsuura USA supported modifying the Lumex Avance-25 for printing magnesium.

References

[1] Walton, Z., Fripp, M., Porter, J., Vargus, G., 2019. Evolution of Frac Plug Technologies–Cast Iron to Composites to Dissolvable, SPE Middle East Oil and Gas Show and Conference, Manama, Bahrain.

[2] Garcilazo Meza, G., Bautista Alarcon, X., Loundy, R., 2020. A Detailed Evaluation of Coiled Tubing Drillouts of Composites and Dissolvable Plugs in Permian Basin and Eagle Ford Fields, SPE/ICoTA Well Intervention Conference and Exhibition, The Woodlands, Texas, USA.

[3] Esmaily, M., Zeng, Z., Mortazavi, N., Gullino, A., Choudhary, S., Derra, T., Benn, F., Delia, F., Muether, M., Thomas, S., 2020. A detailed microstructural and corrosion analysis of an additively manufactured magnesium alloy produced by selective laser melting, 35, p. 101321.

[4] Li, Y., Zhou, J., Pavanram, P., Leeflang, M.A., Fockaert, L.I., Pouran, B., Tümer, N., Schröder, K., Mol, J., Weinans, H., 2018. Additively manufactured biodegradable porous magnesium, Acta biomaterialia 67, p. 378-392.

[5] McGovern, R.K., Weiner, A.M., Sun, L., Chambers, C.G., Zubair, S.M., Lienhard V, J.H., 2014. On the cost of electrodialysis for the desalination of high salinity feeds, Applied Energy 136, p. 649-661.

[6] Elsner, M., Hoelzer, K., 2016. Quantitative Survey and Structural Classification of Hydraulic Fracturing Chemicals Reported in Unconventional Gas Production, Environ. Sci. Technol., 50(7), p. 3290-3314.

[7] American Society for Testing and Materials (Philadelphia, Pennsylvania), 2004. ASTM G31-72: Standard Practice for Laboratory Immersion Corrosion Testing of Metals.

[8] Gibson, I., Rosen, D.W., Stucker, B., 2009. Additive Manufacturing Technologies: Rapid Prototyping to Direct Digital Manufacturing, Springer, Boston.

[9] Hyer, H., Zhou, L., Benson, G., McWilliams, B., Cho, K., Sohn, Y., 2020. Additive manufacturing of dense WE43 Mg alloy by laser powder bed fusion, Additive Manufacturing 33, p. 101123.

[10] Johnston, S., Shi, Z., Atrens, A., 2015. The influence of pH on the corrosion rate of high-purity Mg, AZ91 and ZE41 in bicarbonate buffered Hanks' solution, Corrosion Science 101, p. 182-192.

[11] Sealy, M.P., Karunakaran, R., Ortgies, S., Madireddy, G., Malshe, A.P., Rajurkar, K.P., 2021. Reducing corrosion of additive manufactured magnesium alloys by interlayer ultrasonic peening, CIRP Annals, in press.